Hindawi
Geofluids
Volume 2023, Article ID 3523592, 16 pages
https://doi.org/10.1155/2023/3523592

Research Article

Mechanism and Control Technology of Rockburst Induced by Thick Hard Roof and Residual Coal Pillar: A Case Study

Wenjie Liu,[1,2] **Ke Yang**,[1,2] **Xiang He**,[1,2] **Zhainan Zhang**,[1,2] **and Rijie Xu**[1,2]

[1]*State Key Laboratory of Mining Response and Disaster Prevention and Control in Deep Coal Mines, Anhui University of Science and Technology, Huainan 232001, China*
[2]*National & Local Joint Engineering Research Center of precision coal mining, Anhui University of Science and Technology, Anhui, Huainan 232001, China*

Correspondence should be addressed to Xiang He; xianghe_cumtb@126.com

Received 25 June 2022; Revised 26 October 2022; Accepted 24 November 2022; Published 9 February 2023

Academic Editor: Liang Xin

Rockburst caused by the fracture of thick hard roof and the instantaneous instability of residual coal pillar seriously jeopardize the deep coal mining safety. This study takes Boertai Coal Mine, Shendong, China, as the engineering background, in which dynamic instability mechanisms of the gob-side roadway surrounding rock are analyzed by integrating field research, theoretical analysis, and numerical simulation. The results show that the overlying residual coal pillar, side abutment pressures, and front abutment pressures together induce high static stresses in the surrounding rock of the gob side roadway, with peak values exceeding the in situ stress by one order of magnitude. High stresses accumulated in the goaf-side roadway surrounding rock can easily induce dynamic disaster. With the working face advanced, overburdens are caved in succession, resulting in a continuously decreasing of the overlying residual coal pillar width, once the working face entered the influence area of the residual coal pillar. As the morphology of abutment pressure in the residual coal pillar changes from "unimodal distribution" to "bimodal distribution," the residual coal pillar gradually changes from elastic state to plastic state. When the width of the overlying residual coal pillar is less than the critical width, the thick hard roof and residual coal pillar structure (THRRCPS) lose stability suddenly, resulting in strong dynamic load on the surrounding rock of gob-side roadway. In order to prevent the rockburst of the gob-side roadway under the influence of THRRCPS, regional and local prevention measures are adopted to mitigate the accumulation of stress in the thick hard roof and gob-side roadway surrounding rock by hydraulic fracturing technology and large diameter pressure relief drilling hole.

1. Introduction

As shallow coal resources in eastern China are gradually depleted, the coal mining is shifted to central and western China [1]. Due to large-scale and intensive mining, the mining depth of coal in western China has increased from 100~300 m to 600~750 m in some area [2]. Compared with coal seams in eastern China, those in central and western China are characterized by the overlying strata of hard and thick sandstone. Typical examples are the Yima Mine in Henan, the Datong Mine in Shanxi, the Binchang Mine in Shaanxi, and the Shendong Mine in Inner Mongolia [3]. When shallow coal resources are mined in these regions, many protective coal pillars are reserved to protect surface buildings and reduce surface deformation. After entering the deep mining, the latter part of the mine faces such problems as serious deformation of stope and roadway surrounding rock, severe ground pressure, and frequent occurrence of coal-rock dynamic disasters [4], under the action of the thick hard roof and overlying residual coal pillar, which seriously restricts the coal mining safety and efficiency. Therefore, it is of great significance to study the occurrence regularity and prevention methods of rockburst in these regions.

Successful achievements in mechanisms and prevention methods of rockburst have been reported worldwide [5, 6]. Ortlepp and Stacey [7–9] classified rockbursts into five types: strain burst, buckling, face crush, shear failure, and fault slip burst. In addition, they pointed out that

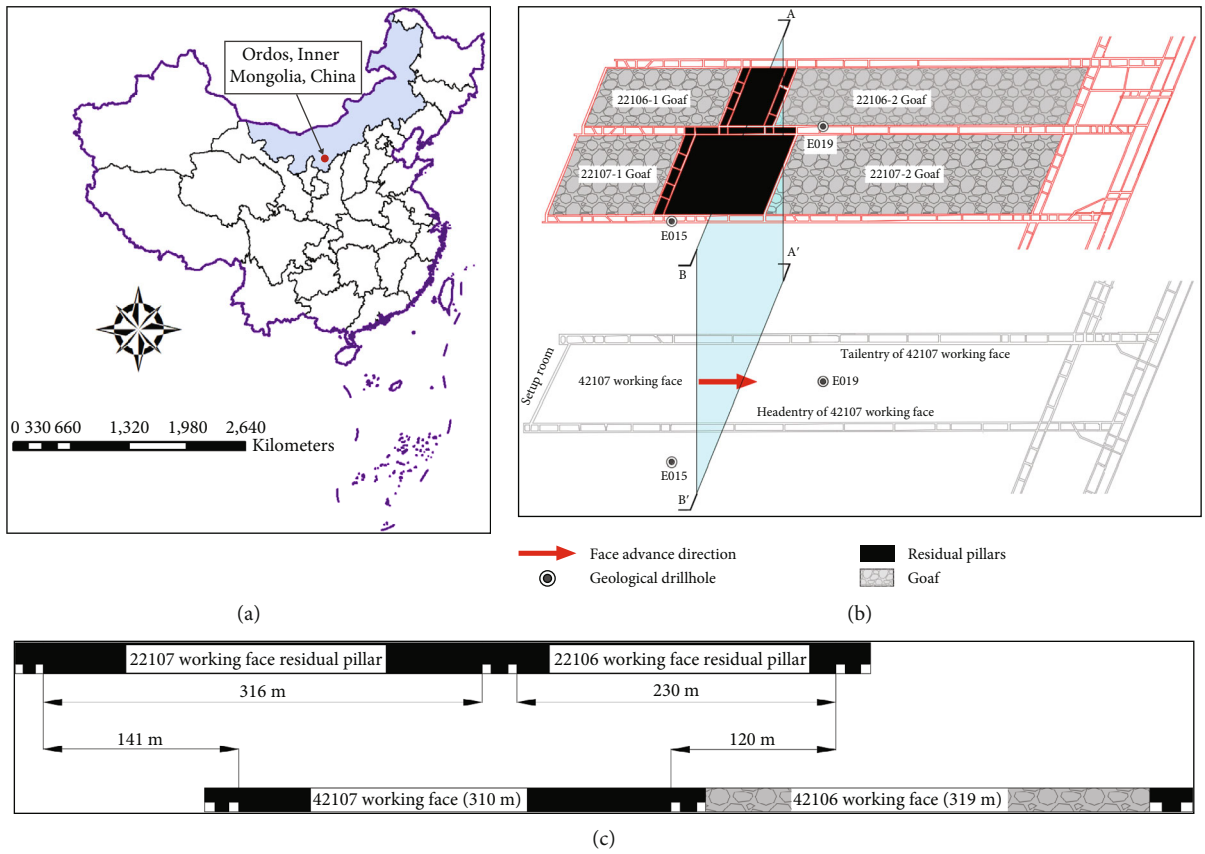

Figure 1: Layout of working faces. (a) Location of Bultai coal mine. (b) Spatial relationship of working faces. (c) AB-A′B′ cross-section drawn.

the rockburst mechanism can be divided into source mechanism and failure mechanism. Dou et al. [10–12] proposed dynamic and static load-imposed rockburst induction mechanism and established a cloud platform for early warning of rockburst. Pan et al. [13, 14] investigated the instability mechanism and conditions of rockburst disturbance response and rockburst roadway antishock energy absorption support. Jiang et al. [15] established three mechanical models of rockburst in the coal mine on the basis of the characteristics of rockburst disasters in coal mines. The large-scale movement of the thick hard roof and the instantaneous instability of the coal pillar cause the rapid release of the accumulated elastic energy, causing serious damage to underground works or ground buildings. In some cases, it may even cause severe casualties and economic losses [16–18]. On March 15, 2013, a rockburst disaster was caused by the sudden collapse of a large area of overhanging thick and hard sandstone in the June Coal Mine. In the accident, twenty-one workers were trapped and five died [19]. On March 27, 2014, six workers were killed in a severe rock explosion caused by the coal mining of the 21032 longwall face giant conglomerate. Hence, many scholars have conducted in-depth research on rockburst mechanisms and prevention technologies induced by the thick hard roof fracturing and coal pillar instability. Cao et al. [20] located areas of high seismic activity in the large residual coal pillar of the working face, using the seismic computed tomography technology and mine earthquake 3D positioning technology to evaluate the rockburst risk when the working face passed the coal pillar. He et al. [21] constructed a theoretical model of rockburst induced by thick hard roof failure and proposed the stress calculation method of support object and coal body induced by the thick hard roof. Six effective methods were proposed to prevent the rockburst induced by thick hard roof fracturing. Ning et al. [22] used the microseismic monitoring technology to study the roof fracturing migration law during coal seam mining under the double-layer thick hard sandstone roof and proposed the deep hole presplitting blasting technology to control the strong dynamic phenomenon caused by large-scale roof fracture. Zhang et al. [23] reported that roof deformation could be controlled by the goaf filling to relieve stress concentration in coal and rock mass. They also determined the thick hard roof fracturing-induced rockburst types under different goaf filling rates. Lai et al. [24] investigated the normal stress evolution law in the coal seam when the underlying working face passed the overlying residual coal pillar. Numerical simulation and physical similarity simulation test were used to reveal the instability mechanism of the overburden structure and specify the rockburst control measures during mining under the residual coal pillar. Kang et al. [25] derived an analytical solution for the abnormal stress

Table 1: Physical and mechanical parameters of the rocks and location of key stratum.

Name	Strata thickness (m)	Tensile strength (MPa)	Elastic modulus (GPa)	Poisson's ratio	Cohesion (MPa)	Friction angle (°)	Bulk density (kg/m^3)	Note
Fine sandstone	38.50	0.42	1.39	0.25	7.30	30.50	2152	
Siltstone	43.50	0.76	2.36	0.27	6.90	29.20	2293	PKS
Sandy mudstone	36.00	1.10	1.45	0.25	5.50	22.60	2330	
Fine sandstone	46.00	1.35	1.62	0.26	6.87	29.90	2219	SKS6
Sandy mudstone	35.50	1.07	1.78	0.26	8.28	26.80	2219	
Siltstone	21.00	2.44	2.05	0.24	10.40	27.40	2350	SKS5
Sandy mudstone	39.50	1.99	1.52	0.31	9.90	25.90	2291	
Fine sandstone	39.50	2.46	3.08	0.25	10.50	24.90	2323	SKS4
Sandy mudstone	11.98	2.76	2.89	0.26	21.70	21.60	2217	
Coal	0.5	1.37	1.99	0.28	19.20	28.20	1274	
Sandy mudstone	8.00	3.36	6.53	0.20	19.70	23.60	2217	
1-1 coal seam	3.00	1.37	1.99	0.28	19.20	28.20	1274	
Sandy mudstone	5.00	4.22	7.24	0.20	19.70	23.60	2111	
1-2 coal seam	1.00	1.37	1.99	0.28	19.20	28.20	1274	
Siltstone	8.00	6.62	6.72	0.24	23.80	22.70	2343	SKS3
Sandy mudstone	16.00	5.24	7.92	0.22	18.90	26.20	2321	
2-2 coal seam	3.50	1.47	1.99	0.28	19.20	24.20	1274	
Sandy mudstone	20.00	4.66	9.60	0.25	23.10	33.30	2350	
Coal	0.5	1.57	1.99	0.28	19.20	28.20	1274	
Sandy mudstone	14.50	5.03	7.59	0.21	24.40	28.30	2363	
Siltstone	22.50	8.03	11.85	0.24	32.40	26.40	2328	SKS2
Sandy mudstone	8.00	5.97	8.56	0.25	27.80	26.60	2403	
Fine sandstone	9.00	9.26	12.48	0.25	35.60	24.50	2301	SKS1
Sandy mudstone	6.00	6.66	10.61	0.25	27.80	26.60	2430	
4-2 coal seam	6.50	1.38	5.44	0.28	19.20	28.20	1274	
Sandy mudstone	8.00	4.73	10.65	0.25	27.80	26.60	2421	
Coal	1.20	4.85	1.99	0.28	19.20	28.20	1274	
Sandy mudstone	2.50	5.66	12.3	0.25	25.60	28.30	2397	
Coal	1.00	1.38	1.99	0.28	19.20	28.20	1274	
Sandy mudstone	25.00	6.04	14.6	0.25	27.70	28.60	2326	
Coal	2.00	1.57	1.99	0.28	19.20	28.20	1274	
Sandy mudstone	21.00	6.71	15.5	0.25	27.70	28.60	2482	
Fine sandstone	22.00	6.60	9.59	0.26	16.60	27.30	2286	
Medium-grained sandstone	5.00	6.13	10.32	0.22	6.56	46.90	2442	

in the strata below residual bearing coal pillars, based on elastic theory and mathematical model for the abutment stress in the residual bearing coal pillars. In terms of rockburst prevention methods, various destressing techniques [26–28] are applied to mitigate burst risks mainly including borehole blasting, destressing boreholes, shotfring, water infusion, and hydraulic fracturing.

The above studies mentioned have greatly promoted the theoretical and practical development of rockburst prevention technologies. However, there are few reports on the gob-side roadway impact instability and stress loading characteristic induced by overburden structure, which results could be applied to the specific mining conditions, e.g., of the Boertai Coal Mine, China. In the case study analysis, it should be taken into account that the occurrence of rockburst is caused by mining disturbances, and the mining overburden structure and the formation of mining stress fields are very important for inducing rockburst. In this study, taking the Boertai Coal Mine as a case study, the mining stress evolution law in working face 42107 and the structural characteristics of overburden in the stope are analyzed. The dynamic instability mechanism of the Boertai Coal Mine's gob side roadway is obtained and corresponding preventive measures are proposed.

2. Project Overview

2.1. Geological Conditions and Mining Layout. The Boertai Coal Mine is located in the southeast of the Ejinholo Banner,

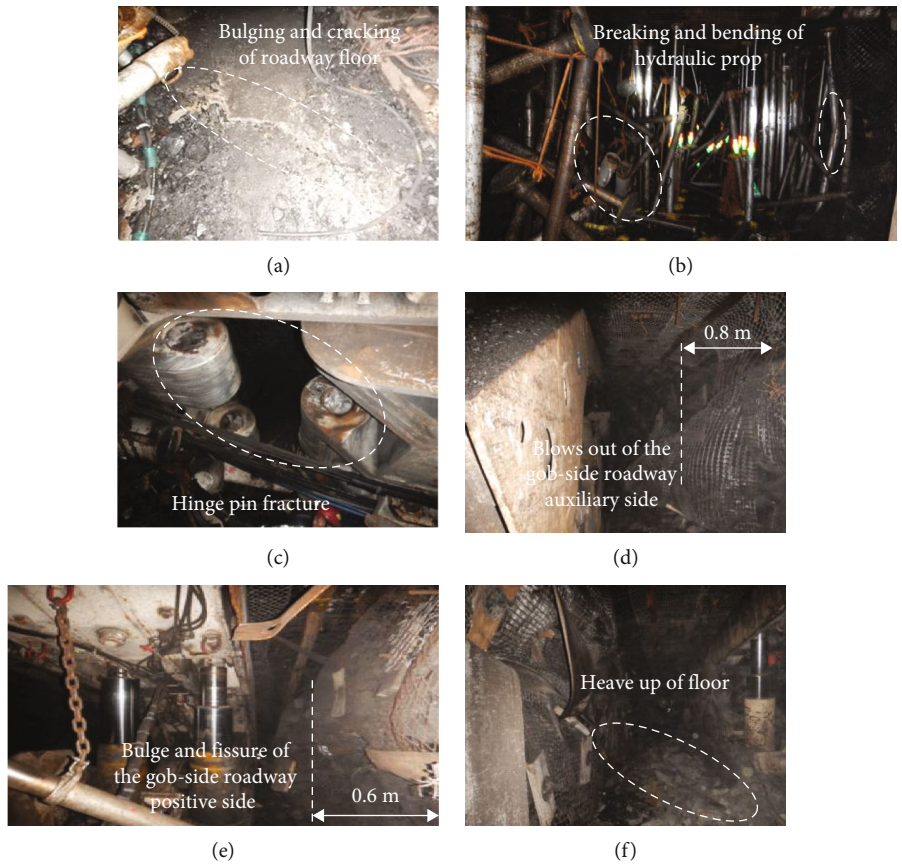

Figure 2: Strong ground pressure accident. (a) Bulge of working face 42105 roadway floor. (b) Breaking of hydraulic prop. (c) Fracture of hinge pin. (d) Bulge of gob-side roadway auxiliary side. (e) Bulge of gob-side roadway positive side. (f) Heave up of floor.

Ordos City, Inner Mongolia, China, as shown in Figure 1(a). The mine design production capacity is 20 million t/a, and the main mining coal seams are 2-2# and 4-2# coal seams. The coal seams have a simple structure and stable occurrence, and the inclination angle of coal seam is 1-3°. The 2-2# coal seam thickness is 0.82~5.80 m, and buried depth is 212~360 m. The 4-2# coal seam thickness is 0.90~7.68 m, and buried depth is 339~460 m. In order to reduce the subsidence and deformation of the railway, when the 2-2# coal seam was mined, a safety coal pillar of 200~400 m has been left in the center of working faces 22106 and 22107. Upon the completed mining of 2-2# coal seam, working face 42107 experienced multiple strong dynamic phenomena. Figures 1(b) and 1(c) show the spatial relationship of different working faces.

Working face 42107 has a length of 4807 m and a width of 300 m, adjacent to 42106 goaf and working face 42108. The chain pillar width is 25 m, the coal seam thickness is 3.46~7.05 m, the average thickness is 6.13 m, and the perpendicular distance from 2-2# coal seam to working face 42107 is about 45~78 m. Working face 42107 is mined by longwall mining with top coal caving. Working face 42107 mining height is 3.6 m, and coal caving height is 2.53 m. The average daily advance speed of working face 42107 is 10 m/d, and the roof is managed by the caving method.

According to the E019# geology columnar of working face 42107 and mechanical parameters of rocks, the key strata theory [29] is used to discriminate the location of the key stratum. As shown in Table 1, the overlying stratum thickness of working face 42107 was 437 m, there exists seven key stratums, and the principal key stratum (PKS) is a siltstone with a distance of 355 m from the 4-2# coal seam and a thickness of 43.5 m. There are two subkey stratums between 4-2# coal seam and 2-2# coal seam, fine sandstone (SKS1) with thickness of 9 m, and siltstone with thickness of 22.5 m (SKS2). The thick and hard roof mentioned in this paper refers to the SKS2.

2.2. Characteristics of the Rockburst Behavior in the Adjacent Working Face. According to onsite statistics and observations, when the adjacent working face of working face 42107 was mined, the rockburst phenomena with different characteristics occurred in the gob-side roadway and the working face. As shown in Figures 2(a) and 2(b), when working face 42105 was advanced to 251.7 m, the ground pressure of the gob-side roadway drastically increased and formed a rockburst. The hydraulic prop in front of the working face, within the range of 20 m, snapped and popped out instantly. The roadway floor had bulging and cracking features. As shown in Figure 2(c), the top beam of the 43#

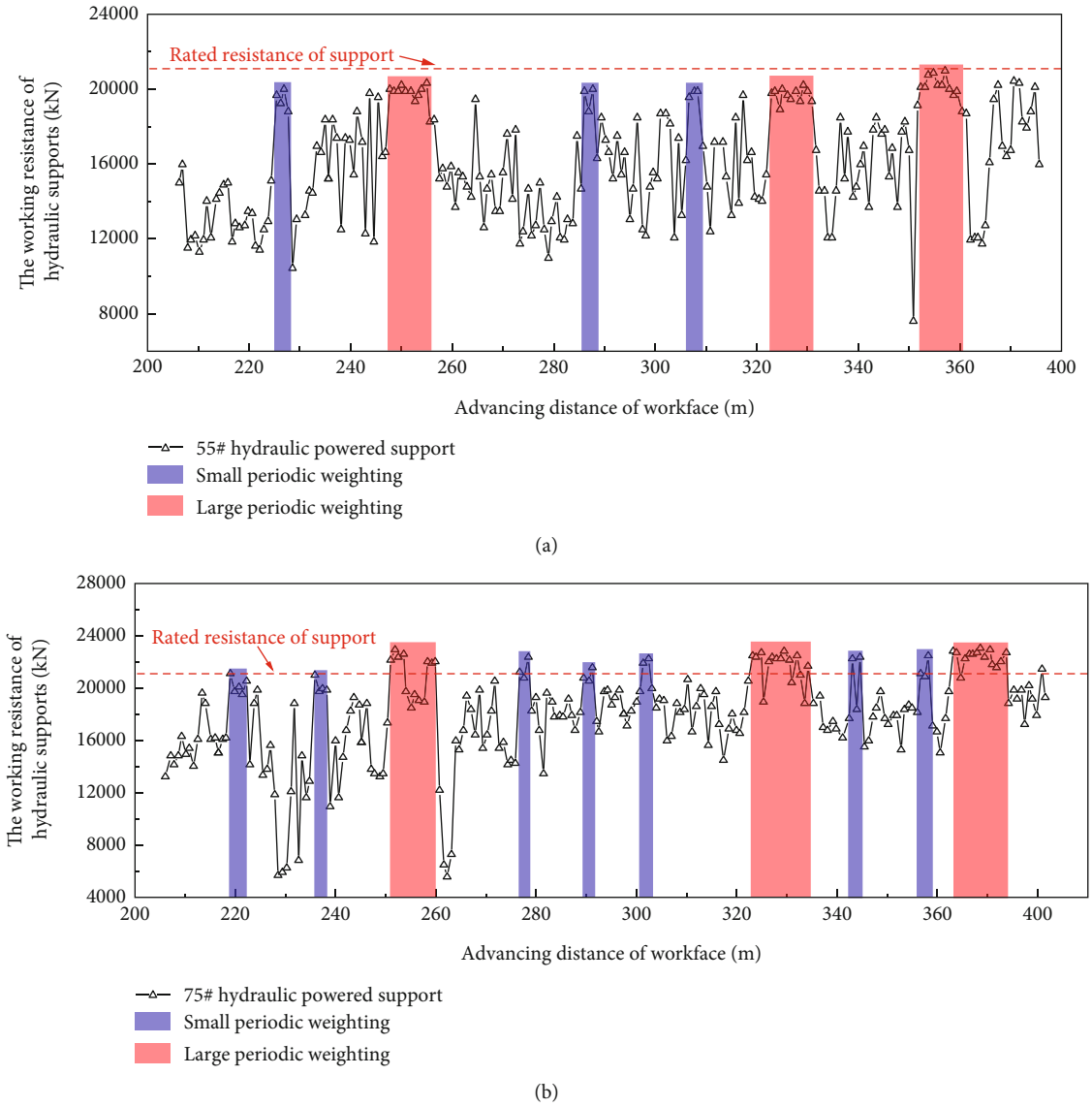

Figure 3: Working resistance of the hydraulic powered support. (a) 55# hydraulic powered support. (b) 75# hydraulic powered support.

Table 2: Stress-strain relationship of double-yield materials.

Strain	Stress (MPa)	Strain	Stress (MPa)
0.01	0.82	0.09	13.97
0.02	1.45	0.10	17.46
0.03	2.80	0.11	21.93
0.04	4.00	0.12	27.89
0.05	5.38	0.13	36.22
0.06	6.99	0.14	48.68
0.07	8.90	0.15	69.36
0.08	11.18	0.16	110.38

hydraulic powered support and shield beam was separated, and the two hinge pins were broken. The horizontal distance between the top beam and the shield beam was 820 mm and, the upper and lower staggered distances were 500 mm.

Table 3: Parameters of double-yield materials in 2-2 goaf.

Density (kg m^{-3})	Bulk modulus (GPa)	Shear modulus (GPa)	Internal friction angle (°)	Dilation angle (°)
1800	19	5	0.2	0.3

The hydraulic prop is classified as a rigid support, its safety valve cannot be opened immediately after the rockburst is applied, resulting in its fracture. In order to solve the hidden danger of hydraulic prop breaking and hurting people, working face 42106 uses an ordinary hydraulic powered support instead of hydraulic prop for the gob-side roadway advanced support. As shown in Figures 2(c)–2(e), when the working face advanced to 140 m, the dynamic load drastically increased, heaving up the floor of gob-side roadway. The auxiliary side of the gob-side roadway bulged about 1.6 m and the positive side by about 0.8 m. The deformation and fracture of

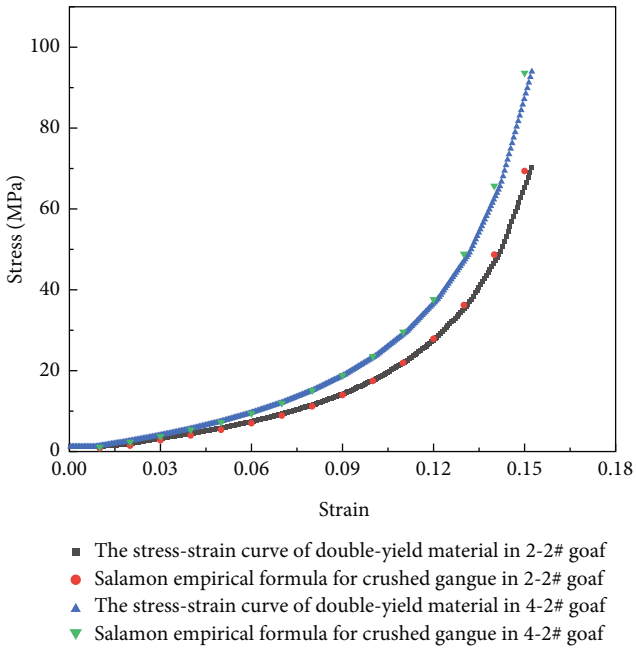

Figure 4: Iteratively fitted results.

Table 4: Parameters of double-yield materials in 4-2 goaf.

Density (kg m^{-3})	Bulk modulus (GPa)	Shear modulus (GPa)	Internal friction angle (°)	Dilation angle (°)
1800	15	1	0.1	0.1

the thick and hard roof led to frequent occurrence of rockburst, which severely jeopardized mining safety. Additionally, the overlying residual coal pillar had a greater impact on the ground pressure of working face 42107.

2.3. The Onsite Mine Pressure Monitoring. In order to obtain the evolution of roof fracturing and reveal the mechanism of rockburst, the working resistance of hydraulic powered support was statistically analyzed in the mining process of working face 42107. As shown in Figure 3, working face 42107 exhibited the characteristics of alternating pressure with large periodic weighting and small period weighting. The rated resistance of the hydraulic powered support is 21000 kN. When the fine sandstone (SKS1) and siltstone (SKS2) underwent synchronized fracturing, the working face has large periodic weighting, with periodic weighting interval about 40~60 m. When the fine sandstone key stratum (SKS1) was fractured while siltstone key stratum (SKS2) was not fractured, small period weighting occurred in the working face, with periodic weighting interval of 15~25 m.

3. The Numerical Simulation

3.1. Determination of Caving Rock Mass Numerical Parameters. After the coal resources were mined, the equilibrium state of the in situ stress was broken, and the stress in the rock mass was redistributed. When there was a free space in the lower part of the rock layer and the stress in the rock layer meet the failure criterion, the rock layer gradually fractured. The caving zone, fractured zone, and continuous deformation zone formed in the overlying strata [27]. The caving zone height can be calculated as follows:

$$H = \frac{m}{K-1}, \tag{1}$$

where H is the caving zone height, m; m is the coal seam mining height, m; and K is the fragmentation coefficient of the rock mass in the caving zone.

After the broken rocks from overlying stratum fell into the goaf, they became gradually compacted under the action of self-weight and overlying strata pressure and then supporting the overburden. During compaction, the strength and elastic modulus of the rock mass in the caving zone gradually grew and tended to the original state. According to the broken rock mass compaction theory [30], the stress-strain relationship of rock mass in the caving zone can be expressed as follows:

$$\sigma_v = \frac{E_0 \varepsilon}{(1-\varepsilon)/\varepsilon_{\max}}, \tag{2}$$

where σ_v is the normal stress in the fractured rock mass of the caving zone, MPa; ε is the normal strain of the fractured rock mass in the goaf; $\varepsilon_{\max}$ is the maximum compressive strain of the fractured rock mass; and E_0 is the initial elastic modulus of the gangue, GPa. Noteworthy is that $\varepsilon_{\max}$ can be derived from the bulking coefficient of rock mass K as follows: $\varepsilon_{\max} = (K-1)/K$, while E_0 can be measured experimentally or calculated as [31]

$$E_0 = \frac{10.39\sigma_{cg}^{1.042}}{K^{7.7}}, \tag{3}$$

where σ_{cg} is the uniaxial compressive strength of the goaf fracturing rock mass, MPa.

It can be obtained from Equation (1) that $K = m/H + 1$. Therefore, in order to obtain the fragmentation coefficient of rock mass in the caving zone, the height of the caving zone should be determined first. Onsite drilling is one of the methods to obtain the exact height of the caving zone, but its realization requires considerable labor and financial resources. Bai et al. [32] obtained the following statistical regression formula of the caving zone height by analyzing the caving zone ranges under various geological conditions in several coal mines in China and the United States:

$$H = \frac{100m}{c_1 m + c_2}, \tag{4}$$

where c_1 and c_2 are parameters closely related to the strata lithology. If the roof above the coal seam was a hard rock stratum, values of $c_1 = 2.1$ and $c_2 = 16$ were used. The calculation shows that when the #2-2 coal seam was mined, the caving zone developed to the bottom of the siltstone key stratum (SKS3) with a height of about 16 m, and the bulking coefficient of the rock mass in the caving zone was 1.22.

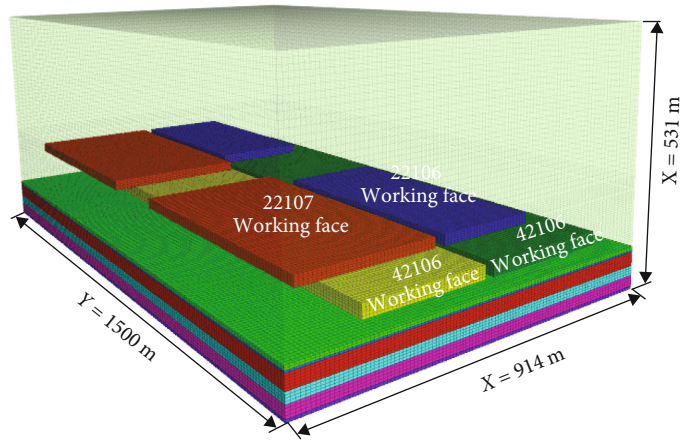

Figure 5: Numerical model of thick hard roof and residual coal pillar structure.

It can be obtained from Equations (1)–(3):

$$\sigma_v = \frac{10.39\sigma_{cg}^{1.042}}{K^{7.7}} \times \frac{\varepsilon}{1-(K/(K-1))\varepsilon}. \quad (5)$$

Referring to the research results of Pappas et al. [30] and taking $\sigma_v = 30$ MPa, the compression stress-strain relationship for the double-yield materials was obtained, as shown in Table 2.

In order to fit the stress-strain relationship of the goaf material to Equation (5), a FLAC unit model was established. The bottom of the model is clamped, the top of the model is free, and the lateral displacements of other four faces are constrained. The vertical velocity was applied to simulate loading on the top surface of the model. The bulk modulus, shear modulus, dilation angle, and internal friction angle were determined by iterative matching. After repeated experiments, the mechanical parameters of the goaf material were obtained and summarized in Table 3, while the matching results were plotted in Figure 4.

Likewise, when working face 42107 was mined, the caving zone height was 22 m. Table 4 lists the double-yield materials' parameters of the rock blocks in the caving zone, while Figure 4 shows the matching results.

3.2. The Numerical Model. The FLAC3D numerical model of the thick hard roof and residual coal pillar structure was established according to the mine's geological data, as shown in Figure 5. The numerical model size was 914 m × 1500 m × 531 m. The model bottom was set as the fixed support boundary, the sides of the model were set as the rolling support boundary, and the upper part of the model simulated to the bedrock layer. According to the ground stress test results [33], the coefficient of horizontal pressure was set at 1.0. Considering the boundary effect, a 60 m wide boundary coal pillar was set around the working face. The elastic-plastic constitutive and the Mohr-Coulomb failure criterion were adopted for the model implementation. Physical and mechanical parameters of each rock layer are listed in Table 1.

4. Results and Analysis

4.1. Trend of the Coal Seam Normal Stress during Mining of Working Face 42107. As shown in Figure 6(a), upon completing the mining of working faces 22106, 22107, and 42106, the normal stress of 4-2# coal seam roof was extracted. The normal stress below the 2-2# goaf is less than the primary rock stress after the mining of working faces 22106 and 22107, indicating that the mining of 2-2# coal seam had a certain pressure relief effect on the 4-2# coal seam. Meanwhile, the stress concentration zone was formed under the 2-2# coal seam residual coal pillar and the chain pillar, but the stress concentration was lower, namely, about 1.5 times of the in situ stress. In this case, a high stress concentration zone was developed in the gob-side roadway surrounding rock of working face 42107. In the influence area of the #2-2 coal seam residual coal pillar, the normal stress in the surrounding rock of the 42107 gob-side roadway was as high as 45~50 MPa, being about twice higher than the normal stress of the nonresidual coal pillar influence area.

The normal stress distributions of the #4-2 coal seam roof under different mining distances are shown in Figures 6(b)–6(g). Affected by the secondary mining, the normal stress in the surrounding rock of working face 42107 gob-side roadway increased again. In the influence area of the residual coal pillar, the normal stress was up to 95 MPa. After working face 42107 entered residual coal pillar influence area, the peak position of normal stress shifted to the side of the 42106 goaf, while the peak value increased slightly, and the shape of normal stress gradually changed from the unimodal state to the straight-line shape. Affected by the overlying residual coal pillar, working face 42107 front abutment pressure and normal stress in the chain coal pillar increased. In the chain coal pillar of 4-2# coal seam, the stress increased about 9 ~ 10 times of the in situ stress. The peak value of the front abutment pressure increased lesser, but the range of the high peak area increased, extending from the middle of the working face to the entire working face. After working face 42107 moved away from the residual coal pillar influence area, the peak value and influence range of the front abutment pressure gradually decreased.

Stress monitoring lines were arranged in the central part of working face 42107 along the inclination direction and

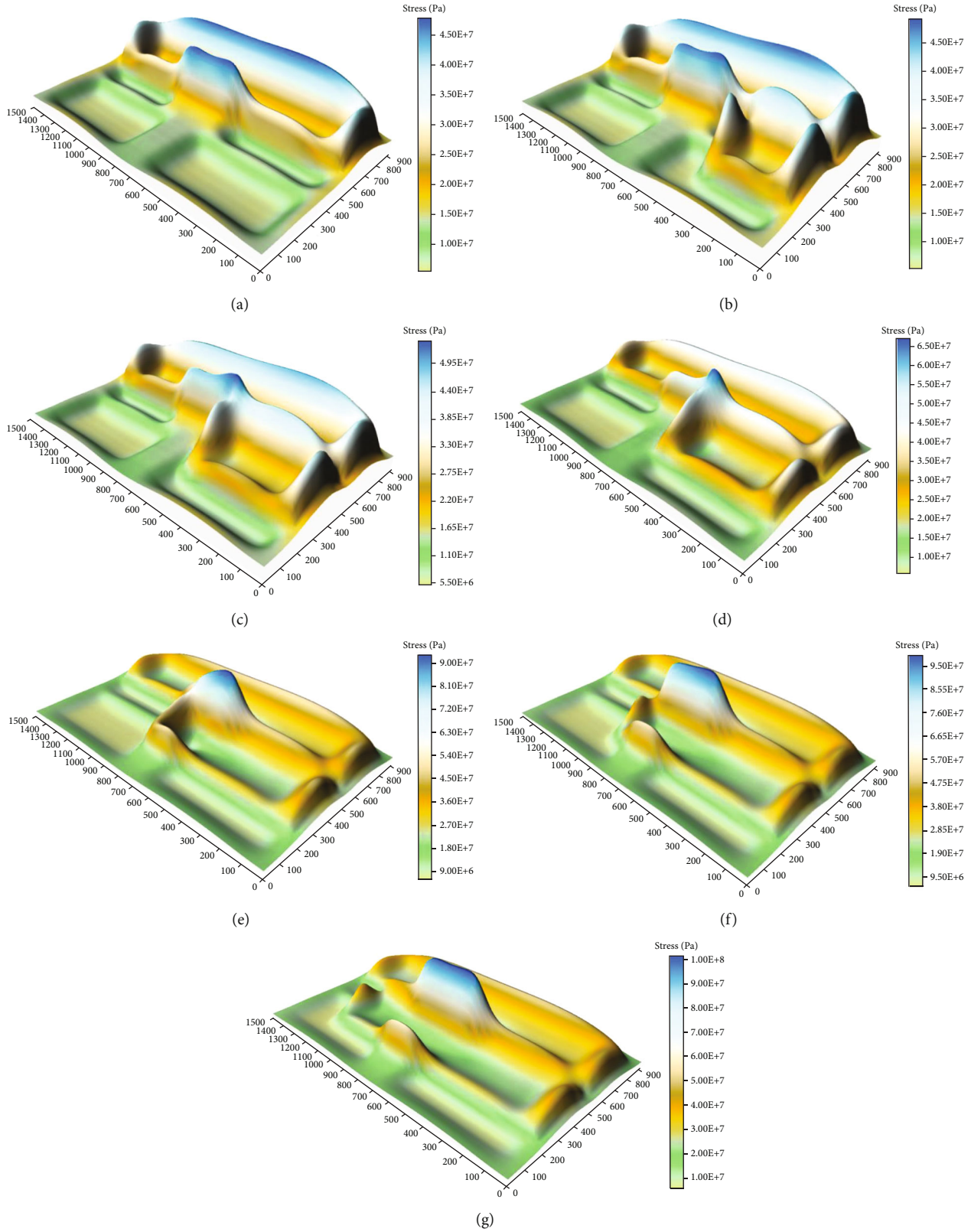

Figure 6: Abutment pressure of 4-2# coal seam. (a) 42107 working face mining 0 m. (b) 42107 working face mining 400 m. (c) 42107 working face mining 550 m. (d) 42107 working face mining 700 m. (e) 42107 working face mining 800 m. (f) 42107 working face mining 1000 m. (g) 42107 working face mining 1200 m.

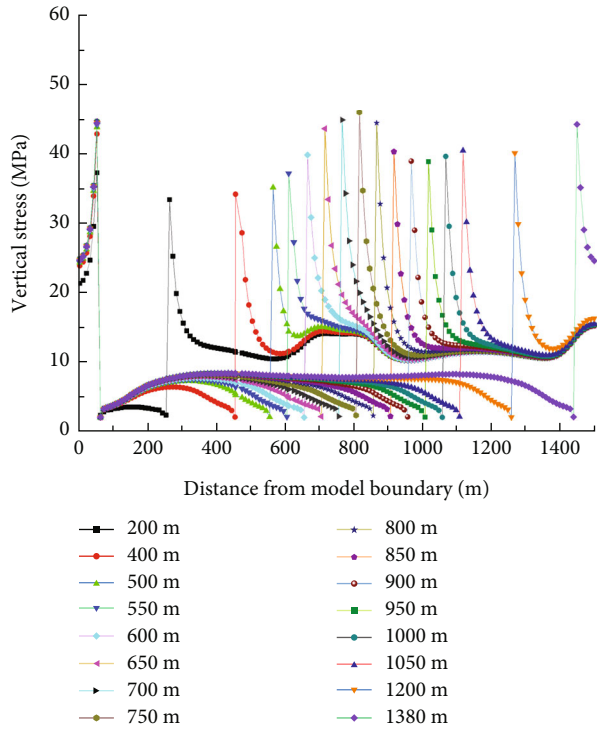

Figure 7: Abutment pressure in the center of 42107 working face.

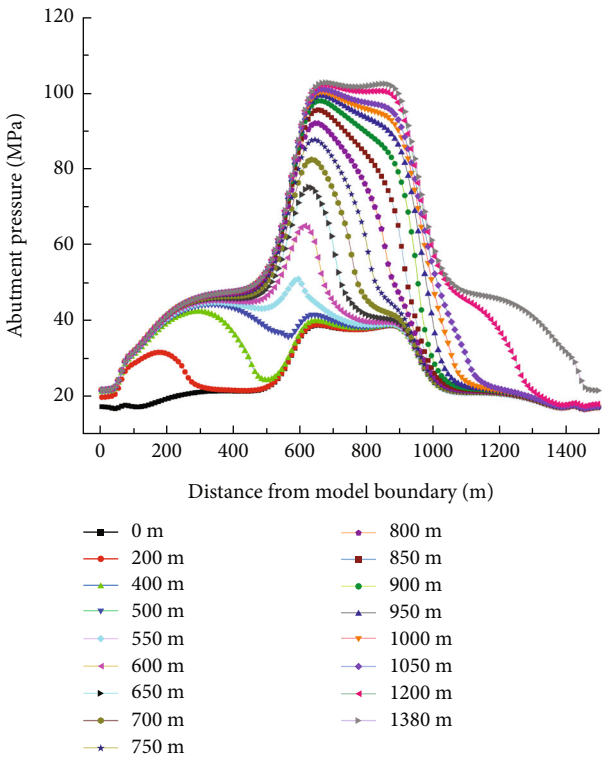

Figure 8: Abutment pressure in the section coal pillar.

chain pillar of 4-2# coal seam to assess the evolution of normal stress in the coal seam at different advancing distances (Figure 7). As shown in Figure 7, with the advancing distance of the working face, the stress in the goaf gradually recovered, and the maximum stress was about 0.8 times of the in situ stress. As shown in Figure 8, after working face 42107 advanced to 400 m, the secondary mining stress and the high stress caused by the residual coal pillar began to superimpose in the gob-side roadway surrounding rock, and the affected range of the residual coal pillar on the 4-2# coal seam was about 600 m. In the nonresidual coal pillar's influence area, under the influence of advance abutment pressure, the gob-side roadway surrounding rock within a range of about 250 m in front of the working face was subjected to high static load. When entering the influence area of the residual coal pillar, the peak value of normal stress in the chain pillar and the range of influence area on 4-2# coal seam increased sharply.

Affected by the overlying residual coal pillar and the mining of working face 42106, during the mining of working face 42107, the gob-side roadway surrounding rock was repeatedly loaded and unloaded by high static load. When working face 42107 approached the residual coal pillar, the stress in the gob-side roadway surrounding rock grew rapidly, while the peak valve of the normal stress increased approximately exponentially (Figure 9).

4.2. Evolution of Thick Hard Roof and Residual Coal Pillar Structure. The deformation and fracturing of the key stratum have a strong influence on the formation and instability of the stope structure and play a controlling role on the dynamic disaster. Surface observations show that the surface cracking and "step-like" subsidence occurred after the 4-2# coal seam mining, suggesting that all key stratum experienced fracture, rotation, and subsidence. According to the work resistance of hydraulic powered support, the near-field key strata, namely, SKS1 and SKS2, play a major role in controlling the appearance of ground pressure in working face 42107.

According to the mine pressure theory [27], two basic morphological types may appear after the key stratum fracturing in the stope, namely, cantilever beam structure and Voussoir beam structure. These two structures determine the size of the working face pressure and degree of disaster. The main influencing factors of the structure formed after the key stratum fracturing are mining height and the distance from key stratum to the coal seam. That is, after key stratum fracturing, the rotation of broken rocks may exceed the maximum rotation of the stable structure. According to previous studies [34], the rotation degree Δ_J of the broken rocks of the key stratum and the maximum rotation degree $\Delta_{\max}$ required to form the cantilever beam structure are as follows:

$$\Delta_J = m - (K_S - 1)h_L, \tag{6}$$

$$\Delta_{\max} = h - L\sqrt{\frac{2(q_0 + \gamma h)}{[\sigma]}}, \tag{7}$$

where m is the coal seam mining height, K_S is the comprehensive bulking coefficient of low-level caving blocks between the coal seam and the key stratum bottom, h_L is the height of the

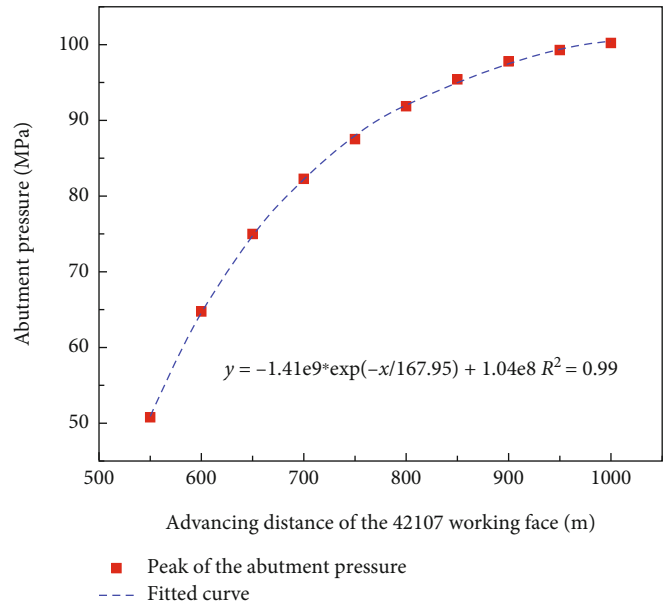

Figure 9: Relation between peak value of abutment pressure in the section coal pillar and mining distance of working face.

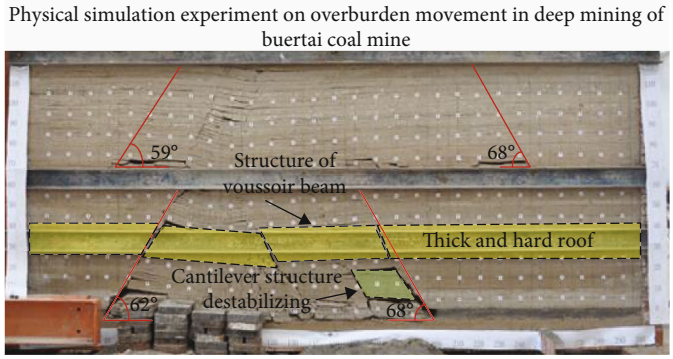

Figure 10: Results of physical simulation experiment.

key stratum measured from the coal seam, L is the fracturing step of the key stratum, q_0 is the overlying strata load by the key stratum rock beam, γ and h are the specific weight and thickness of the key stratum, respectively, and $[\sigma]$ is the key stratum fracturing the compressive strength of the rock block, typically $[\sigma] = (0.3 \sim 0.4)[\sigma_h]$, where $[\sigma_h]$ is the extreme compressive strength of the key stratum.

The formation condition of the cantilever beam structure is $\Delta_J \geq \Delta_{max}$; otherwise, the Voussoir beam structure is formed. Mining practice shows that when the key stratum is far from the coal seam, a Voussoir beam structure is usually formed. On the contrary, if the coal seam mining height is larger and the key stratum is closer to the coal seam, the cantilever beam structure is easy to form. Working face 42107 had a mining height of 6.5 m, and the vertical distance between the SKS1 and 4-2# coal seam was only 6 m. Therefore, the cantilever beam structure will be formed after SKS1 fracturing.

Based on the occurrence characteristics of stratum in working face 42107, the structure type formed by SKS2 broken rock was analyzed. According to the onsite mining practice, the fracture height of the overlying stratum after the 4-2# coal seam mining was about 40~60 m. That is, the fracture height of overlying stratum in the vertical direction of 4-2# coal seam could run through the 2-2# goaf, with $q_0 = 2.31$ MPa. According to the analysis of the onsite support pressure data, the cycle fracturing distance of SKS2 was about 50 m. Other parameters were as follows: $m = 6.5$ m, $K_s = 1.25$, $h_L = 20$ m, $g = 26$ kN/m^3, and $[\sigma] = 40$ MPa. Substituting Equations (1) and (2), we get $J = 1.5$ m, $\Delta_J = 1.5$ m, and $\Delta_{max} = 2.34$, satisfying the inequality $\Delta_J < \Delta_{max}$ and suggesting that during working face 42107 mining, the Voussoir beam structure could be formed when SKS2 was fractured.

As shown in Figure 10, physical simulation experiment revealed that periodic fracturing distance of SKS1 is about 20 m, and that of SKS2 is about 50 m [35], which was consistent with the periodic weighting interval. Broken rocks generated by the fractured SKS2 formed the Voussoir beam structure, while broken rocks generated by the fractured SKS1 formed cantilever beam structure. The physical simulation experiment results well matched the above theoretical

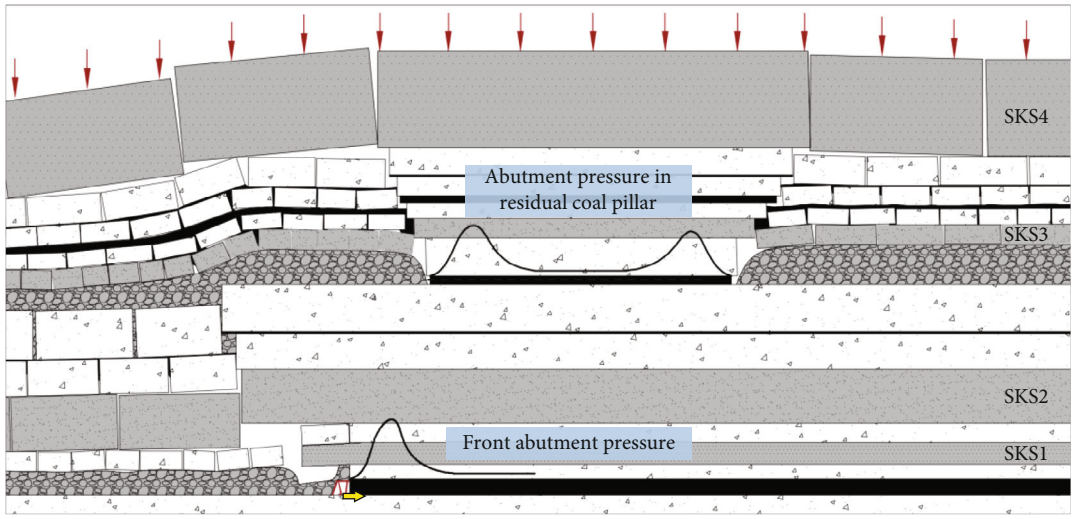

(a)

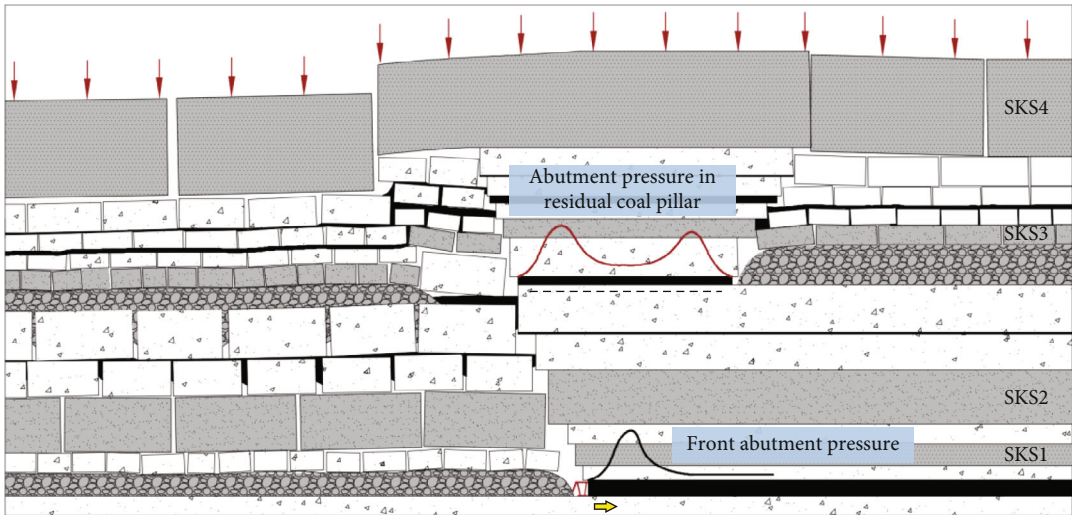

(b)

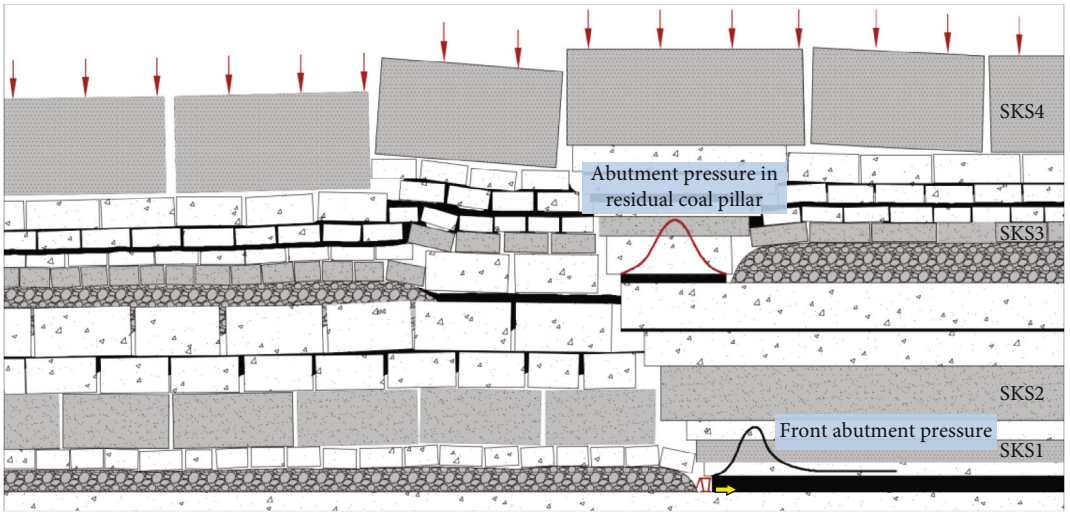

(c)

Figure 11: Evolution of THRRCPS and abutment pressure of section coal pillar.

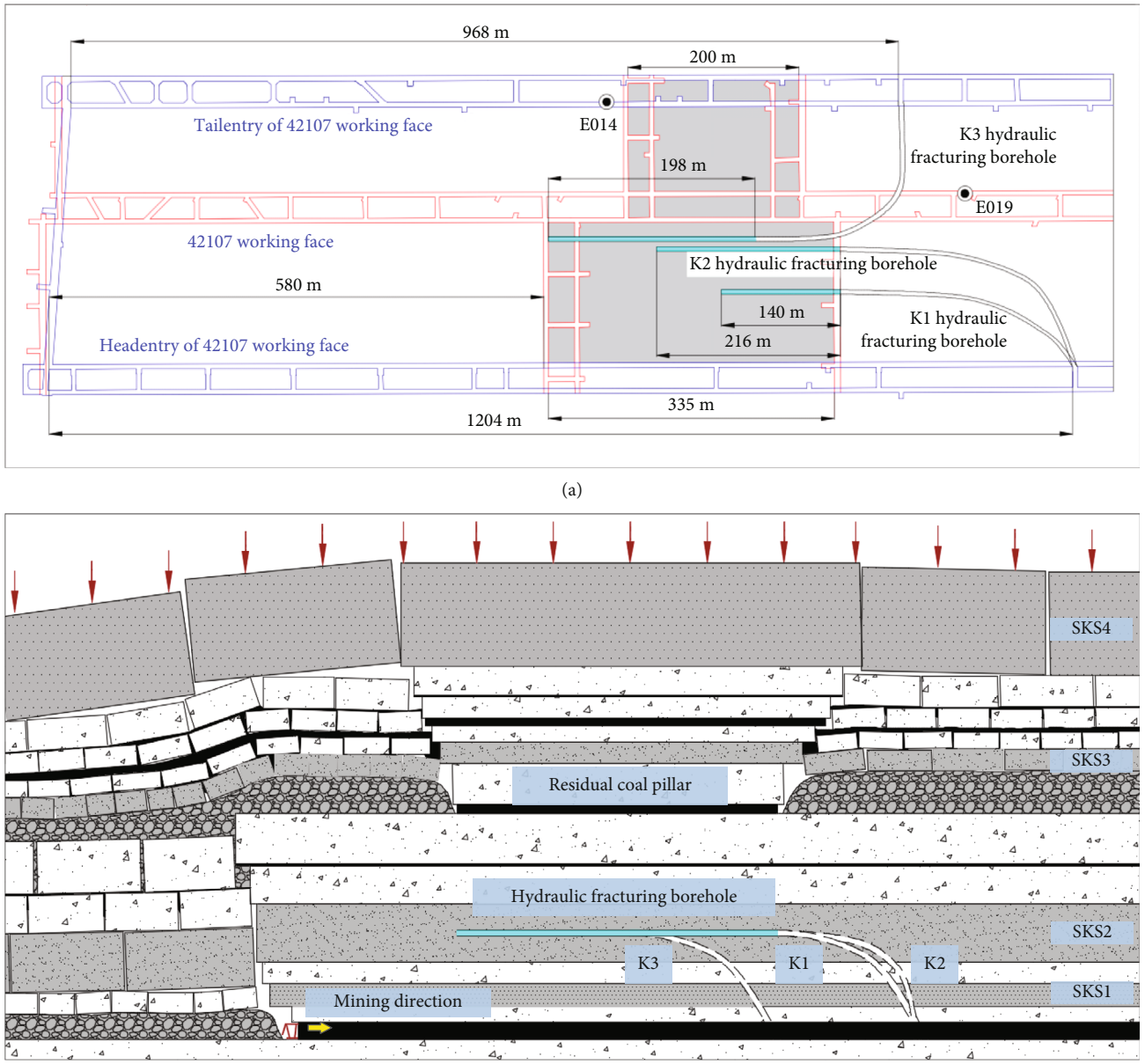

Figure 12: Hydraulic fracturing scheme: (a) plane graph and (b) section graph.

analysis results. Therefore, SKS2 and SKS1 of working face 42107 formed "Voussoir-cantilever" structure after fracturing.

In order to further explore the formation and instability characteristics of the "thick hard roof-residual coal pillar" structure, the evolution of the residual coal pillar pressure, and its stability status under the mining of working face 42107 was analyzed. Typical state of the "thick hard roof-residual coal pillar" structure in the mining process of working face 42107 are shown in Figures 11(a)–11(c).

As shown in Figure 11(a), with advancing of working face 42107, the stratum above the coal seam gradually collapsed. The overburden gravity originally borne by the coal seam was transferred to the surrounding rock mass, forming the front abutment pressure in front of the working face. When the working face advanced by a certain distance, the key stratum reached its extreme fracturing distance, and the support pressure reached its peak value.

When the broken of SKS2 induced the instability of cantilever beam structure, a large amount of elastic energy stored in the rock was released and the peak value of front abutment pressure was reduced. In this case, working face 42107 was far away from the residual coal pillar of 2-2 coal seam and the residual coal pillar width was large. The coal pillar was in a completely elastic state, the middle of the coal pillar was in a state of in situ stress, and the coal pillar was relatively stable. However, as the working face continued to advance, the thick hard roof underwent periodic fracturing, and the "Voussoir beam-cantilever beam" structure experienced periodic instability. As working face 42107 approached the residual coal pillars of the #2-2 coal seam,

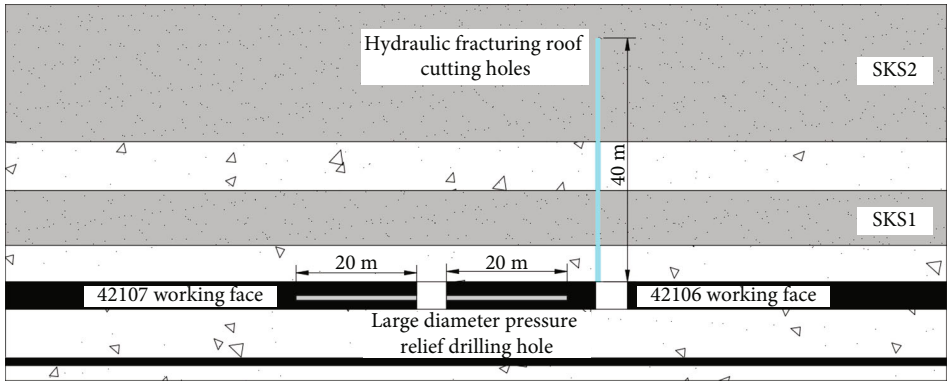

Figure 13: Destressing method of the 42107 tailentry surrounding rock.

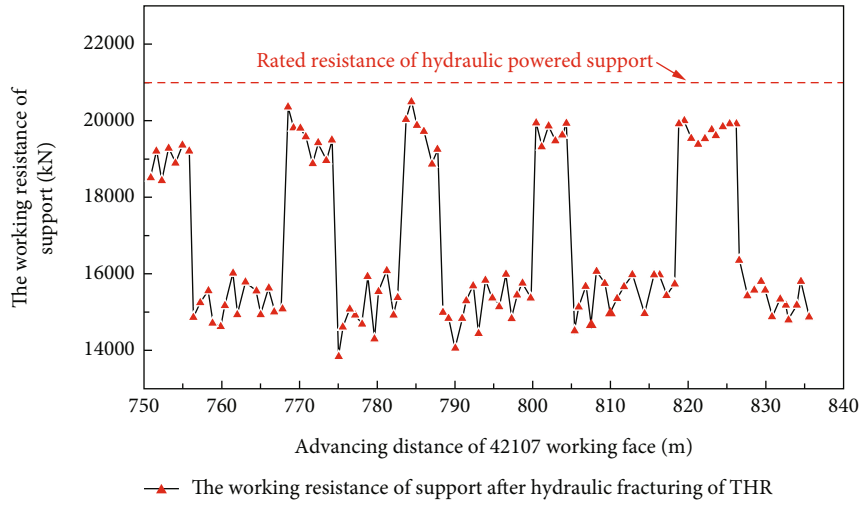

Figure 14: Periodic weighting interval of working face 42107 after hydraulic fracturing of thick hard roof.

the accumulation of a large amount of energy occurred in the thick hard roof, affecting the fracturing of the thick hard roof and the stability of the "Voussoir beam-cantilever beam" structure. On the other hand, the overlying strata will undergo fracturing after the thick roof fracturing, resulting in the reduced of the coal pillar width and the superimposition of abutment pressure. As shown in Figure 11(b), the edge of the residual coal pillar is in plastic state, the middle of the coal pillar is in elastic state, and the residual coal pillar is still in stable state. When the residual coal pillar width is smaller than the influence range of the abutment pressure, the superposition effect of the abutment pressure is remarkable. The abutment pressure in the residual coal pillar evolves from the unimodal distribution pattern to the bimodal distribution pattern. The range of the plasticity zone in the residual coal pillar begins to expand, and the coal pillar is under the critical instability state [36]. In this case, it is easy to cause the impact instability of "thick hard roof - residual coal pillar" structure.

5. Rockburst Mechanism and Control Measures

5.1. Rockburst Mechanism under the Effect of THRRCPS. Under the action of overlying load and self-weight, the key stratum is exposed to bending, fracturing, and collapse, which is accompanied with the accumulation and release of energy. When the overhang area of SKS2 increase to the extreme span, compound fracture occurred in the SKS1 and SKS2, with the accumulated elastic energy being suddenly released. The strong vibration generated by this fracturing exerts a dynamic load on the coal seam. The rock stress around the working face becomes significantly increased, and strong working face pressure is generated. On the other hand, when working face 42107 under the residual coal pillar influence area, the width of the residual coal pillar keeps decreasing after SKS2 and SKS1 fractured. The stress concentration in the residual coal pillar and high energy concentration area formed in working face 42107 below the residual coal pillar. When the residual coal pillar is unstable, a large range of overburden failure, and the dynamic load will lead to the instability and damage of the coal and rock system.

As follows from the previous discussion, the increase of the thick and hard roof overhang area and the reduced of the residual coal pillar width will form a high static load concentration area in working face 42107. The fracture of the thick hard roof and the instability of residual coal pillar will release high dynamic stresses, providing the energy for rockburst. Under the superposition of dynamic and static loads,

coal and rock mass reach their ultimate bearing strength, which induces the occurrence of rockburst.

5.2. Control Measure of Rockburst under the Effect of THRRCPS. According to the mechanism of rockburst under the effect of THRRCPS, the control of thick hard roof and residual coal pillar should be strengthened in the working face of multicoal seam mining. On the one hand, the overhang area of the thick hard roof should be reduced. On the other hand, the stress concentration in the coal seam below the residual coal pillar should be eliminated. Hence, reducing stress concentration and the stress transfer efficiency are considered expedient.

As shown in Figure 12, before the mining of working face 42107, three underground directional drilling holes K1, K2, and K3 were constructed in the headentry and tailentry of working face 42107 to conduct hydraulic fracturing on the thick hard roof (SKS2) below the residual coal pillar. Large overhanging of the thick hard roof was avoided, the periodic weighting interval of the thick hard roof was controlled, and the effective accumulation of the stress in the THRRCPS was cut off. During the mining of working face 42107, the surrounding rock of 42107 tailentry will be relieved by hydraulic fracturing roof cutting technology and large diameter pressure relief drilling hole. Thus, the transfer efficiency of the energy released to the working face will be reduced when THRRCPS become destabilized.

As shown in Figure 13, aimed at cutting off the hanging roof in the 42106 goaf and reducing the stress of 42107 tailentry surrounding rock, hydraulic roof cutting holes are arranged in the 42106 headentry. The drilling direction is perpendicular to the coal seam roof, the hole depth is 40 m, and the spacing between the two holes along the working face is 10 m. Before the mining of 42107 working face, large-diameter boreholes are arranged in the 42107 tailentry. The drilling direction is perpendicular to the coal wall toward the coal pillar and solid coal. The borehole is 1.5 m away from the roadway floor, 20 m deep, and 113 mm in diameter. The spacing between adjacent pressure relief boreholes along the working face is 1.5 m.

After horizontal directional drilling is adopted to conduct hydraulic fracturing on the thick hard roof, the working resistance of hydraulic powered support in 42107 working face is shown in Figure 14. It can be seen from the Figure 14 that the periodic weighting interval of 42107 working face is reduced to 16.9 m, and the average working resistance of the support is 19599 kN, which is less than the rated resistance of the support (21000 kN), and the occurrence of rockburst in working face 42107 is well controlled.

6. Conclusions

The instantaneous instability of the THRRCPS caused significant dynamic load on working face 42107. The field research, theoretical analysis, and numerical simulation results make it possible to draw the following conclusions:

(1) After working face 42107 entered the influence area of the overlying residual coal pillar, gob-side roadway surrounding rock was affected by the overlying residual coal pillar static load, as well as the side and front abutment pressure static loads, which implied the stress conditions for the manifestation of rockburst and the accumulation of a large amount of energy in the chain pillar

(2) With the continuous advancement of working face 42107, the thick hard roof was fracturing step by step, and the residual coal pillar width gradually decreased. When the residual coal pillar width reached the critical value, the residual coal pillar became unstable instantaneously, easily causing the large-scale migration of the overburden. The dynamic load will lead to the instability and fracture of the coal and rock system and induce rockburst

(3) Based on the mechanism of rockburst induced by the destabilization of THRRCPS, a governance measure is recommended to eliminate the stress concentration and reduce the dynamic stress transfer efficiency. The hydraulic fracturing was used to reduce the accumulation of stress in the thick and hard roof before mining. During the mining period, the coal seam deep-hole loosening blasting and large-diameter pressure relief drilling technology was used to reduce the transmission efficiency of dynamic stress to the working face when THRRCPS is unstable

Data Availability

The data used to support the findings of this study are included within the article.

Conflicts of Interest

The submission has been received explicitly from all co-authors. And authors whose names appear on the submission have contributed sufficiently to the scientific work and therefore share collective responsibility and accountability for the results.

Acknowledgments

This work was supported by the graduate research project of Universities in Anhui Province, China (YJS20210390), National Natural Science Foundation of China (U21A20110), and Collaborative Innovation Project of Anhui Universities (GXXT-2019-029).

References

[1] T. B. Zhao, Y. C. Yin, and Y. L. Tan, "Safe mining and new prediction model in coal seam with rock burst induced by roof," *Disaster Advances*, vol. 5, no. 4, pp. 961–965, 2012.

[2] Y. X. Zhao, J. L. Zhou, and W. G. Liu, "Characteristics of ground pressure and mechanism of coal burst in the gob side roadway at Xinjie deep mining area," *Journal of China Coal Society*, vol. 45, no. 5, pp. 1595–1606, 2020.

[3] J. He, L. M. Dou, Z. L. Mu, A. Y. Cao, and S. Y. Gong, "Numerical simulation study on hard-thick roof inducing rock burst in coal mine," *Journal of Central South University*, vol. 23, no. 9, pp. 2314–2320, 2016.

[4] L. M. Dou and X. Q. He, *Theory and Technique on Rockburst Prevention*, China University of Mining and Technology Press, 2001.

[5] Y. Xue, J. Liu, P. G. Ranjith, F. Gao, H. Xie, and J. Wang, "Changes in microstructure and mechanical properties of low-permeability coal induced by pulsating nitrogen fatigue fracturing tests," *Rock Mechanics and Rock Engineering*, vol. 55, no. 12, pp. 7469–7488, 2022.

[6] Y. Xue, P. G. Ranjith, Y. Chen, C. Cai, F. Gao, and X. Liu, "Nonlinear mechanical characteristics and damage constitutive model of coal under CO_2 adsorption during geological sequestration," *Fuel*, vol. 331, article 125690, 2023.

[7] W. D. Ortlepp and T. R. Stacey, "Rockburst mechanisms in tunnels and shafts," *Tunnelling and Underground Space Technology*, vol. 9, no. 1, pp. 59–65, 1994.

[8] W. Ortlepp, *Rock Fracture and Rockbursts: An Illustrative Study*, South African Institute of Mining and Metallurgy, Johannesburg, 1997.

[9] W. D. Ortlepp, "RaSiM comes of age—a review of the contribution to the understanding and control of mine rockbursts," in *RaSiM6: Proceedings of the Sixth International Symposium on Rockburst and Seismicity in Mines Proceedings*, pp. 9–11, Perth, Western Australia, 2005.

[10] L. M. Dou, C. P. Lu, Z. L. Mou, Y. H. Qin, and J. M. Yao, "Intensity weakening theory for rockburst and its application," *Journal of China Coal Society*, vol. 6, pp. 690–694, 2005.

[11] L. M. Dou, J. He, A. Y. Cao, S. Y. Gong, and W. Cai, "Rock burst prevention methods based on theory of dynamic and static combined load induced in coal mine," *Journal of China Coal Society*, vol. 40, no. 7, pp. 1469–1476, 2015.

[12] L. M. Dou, S. C. Wang, S. Y. Gong, W. Cai, and X. L. Li, "Cloud platform of rock-burst intelligent risk assessment and multi-parameter monitoring and early warning," *Journal of China Coal Society*, vol. 45, no. 6, pp. 2248–2255, 2020.

[13] J. F. Pan, Q. X. Qi, S. H. Liu, S. W. Wang, W. T. Ma, and X. C. Hang, "Characteristics types and prevention and control technology of rock burst in deep coal mining in China," *Journal of China Coal Society*, vol. 45, no. 1, pp. 111–121, 2020.

[14] Y. S. Pan, Q. X. Qi, A. W. Wang et al., "Theory and technology of three levels support in bump-prone roadway," *Journal of China Coal Society*, vol. 43, no. 8, pp. 2091–2098, 2018.

[15] Y.-d. Jiang, Y.-s. Pan, F.-x. Jiang, L.-M. Dou, and Y. Ju, "State of the art review on mechanism and prevention of coal bumps in China," *Journal of China Coal Society*, vol. 39, no. 2, pp. 205–213, 2014.

[16] S. J. Gibowicz and A. Kijko, *An Introduction to Mining Seismology*, Academic Press, San Diego, 1994.

[17] L. Dou, T. Chen, S. Gong, H. He, and S. Zhang, "Rockburst hazard determination by using computed tomography technology in deep workface," *Safety Science*, vol. 50, no. 4, pp. 736–740, 2012.

[18] J. He, L. Dou, S. Gong, J. Li, and Z. Ma, "Rock burst assessment and prediction by dynamic and static stress analysis based on micro-seismic monitoring," *International Journal of Rock Mechanics and Mining Sciences*, vol. 93, pp. 46–53, 2017.

[19] C.-P. Lu, G.-J. Liu, Y. Liu, N. Zhang, J.-H. Xue, and L. Zhang, "Microseismic multi-parameter characteristics of rockburst hazard induced by hard roof fall and high stress concentration," *International Journal of Rock Mechanics and Mining Sciences*, vol. 76, pp. 18–32, 2015.

[20] A. Y. Cao, L. M. Dou, C. B. Wang, X. X. Yao, J. Y. Dong, and Y. Gu, "Microseismic precursory characteristics of rock burst hazard in mining areas near a large residual coal pillar: a case study from Xuzhuang coal mine, Xuzhou, China," *Rock Mechanics and Rock Engineering*, vol. 49, no. 11, pp. 4407–4422, 2016.

[21] J. He, L. M. Dou, A. Y. Cao, S. Y. Gong, and J. W. Lü, "Rock burst induced by roof breakage and its prevention," *Journal of Central South University*, vol. 19, no. 4, pp. 1086–1091, 2012.

[22] J. Ning, J. Wang, L. Jiang, N. Jiang, X. Liu, and J. Jiang, "Fracture analysis of double-layer hard and thick roof and the controlling effect on strata behavior: a case study," *Engineering Failure Analysis*, vol. 81, pp. 117–134, 2017.

[23] J. Zhang, B. Li, N. Zhou, and Q. Zhang, "Application of solid backfilling to reduce hard-roof caving and longwall coal face burst potential," *International Journal of Rock Mechanics and Mining Sciences*, vol. 88, pp. 197–205, 2016.

[24] X. Lai, H. Xu, J. Fan et al., "Study on the mechanism and control of rock burst of coal pillar under complex conditions," *Geofluids*, vol. 2020, Article ID 8847003, 19 pages, 2020.

[25] J. Kang, W. Shen, J. Bai et al., "Influence of abnormal stress under a residual bearing coal pillar on the stability of a mine entry," *International Journal of Mining Science and Technology*, vol. 27, no. 6, pp. 945–954, 2017.

[26] A. T. Iannacchione and S. C. Tadolini, "Occurrence, predication, and control of coal burst events in the US," *International Journal of Mining Science and Technology*, vol. 26, no. 1, pp. 39–46, 2016.

[27] H. He, L. Dou, J. Fan, T. Du, and X. Sun, "Deep-hole directional fracturing of thick hard roof for rockburst prevention," *Tunnelling and Underground Space Technology*, vol. 32, pp. 34–43, 2012.

[28] C. Wei, C. Zhang, I. Canbulat, A. Cao, and L. Dou, "Evaluation of current coal burst control techniques and development of a coal burst management framework," *Tunnelling and Underground Space Technology*, vol. 81, pp. 129–143, 2018.

[29] M. G. Qian, X. X. Miao, and J. L. Xu, "Theoretical study of key stratum in ground control," *Journal of China Coal Society*, vol. 21, no. 3, pp. 225–230, 1996.

[30] D. M. Pappas and C. Mark, *Behavior of Simulated Longwall Gob Material*, US Department of the Interior, Bureau of Mines, 1993.

[31] H. Yavuz, "An estimation method for cover pressure re-establishment distance and pressure distribution in the goaf of longwall coal mines," *International Journal of Rock Mechanics and Mining Sciences*, vol. 41, no. 2, pp. 193–205, 2004.

[32] M. Bai, F. Kendorski, and R. Van, "Chinese and North American high-extraction underground coal mining strata behavior and water protection experience and guidelines," *Proceedings of the 14th International Conference on Ground Control in Mining*, , pp. 209–217, West Virginia University press, Morgantown, 1995.

[33] D. H. Yang, *Research on In-Situ Stress Measurement Method and Application Based on Kaiser Effect of Drilling Core*, China University of Mining and Technology, Beijing, 2019.

[34] M. G. Qian, P. W. Shi, and J. L. Xu, *Ground Pressure and Strata Control*, China University of Mining and Technology Press, Xuzhou, 2010.

[35] K. Yang, X. Chi, W. Liu, L. Dou, and Z. Wei, "Strong ground pressure mechanism and control at the longwall top coal caving with a single key stratum in goaf," *Shock and Vibration*, vol. 2020, Article ID 8835101, 12 pages, 2020.

[36] M. Zhang, Y. H. Cheng, L. Wang, F. Jiang, and L. Qi, "Structure model and stability research of thick hard strata-coal pillar in shallow-buried re-mined panels," *Chinese Journal of Rock Mechanics and Engineering*, vol. 38, no. 1, pp. 87–100, 2019.